

Large-Eddy Simulation at Scales Ranging from Laboratory Channels to Valley Winds in the Atmosphere: Subfilter-scale Model Effects

F. K. Chow, University of California, Berkeley, Civil and Environmental Engineering, Berkeley, CA 94720-1710 USA

R. L. Street, Stanford University, Environmental Fluid Mechanics Laboratory, Stanford, CA 94305-4020 USA

Large-eddy simulations of a number of flows, ranging in size from small to large, are reviewed in the context of the models used to represent those flow motions that are not fully resolved, i.e., the subfilter scales. It is observed that the requirements for representation of these smaller scales changes as the scale and boundary conditions of the simulated flow change. This paper summarizes and explains the reasons for our observations.

1. Introduction

Large-eddy simulation [LES] employs a spatial filter to separate the small scales from the large scales. The large eddies are explicitly calculated, while the effects of the smaller eddies on the larger ones must be modeled. Application of the spatial filter [e.g., a top-hat or Gaussian filter] creates a set of equations for the resolved or filtered field which contains a subfilter-scale [SFS] stress term that is reconstructed and/or modeled.

Carati et al. (2001) presented a velocity partitioning scheme that is useful for our understanding of the SFS terms. Figure 1 shows a schematic of a typical energy spectrum from a turbulent flow field. The application of a filter and a discretization operator (needed to solve the LES equations on a discrete grid) separates the spectrum into three parts. The low wave numbers are filtered and well resolved on the grid. They are contained in the velocity \bar{u} , where the tilde operator represents the effect of discretization and the overbar represents an explicit smooth filter. The middle portion (shaded) represents subfilter-scale

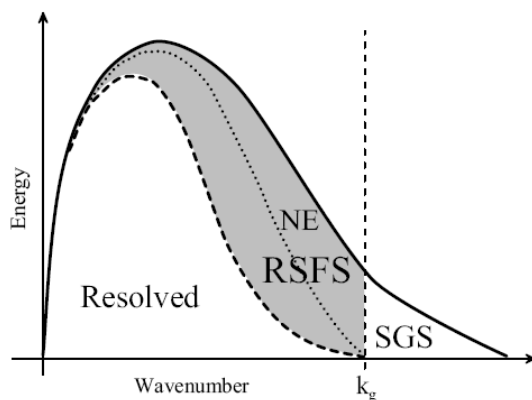


Fig. 1 Schematic of velocity energy spectrum showing partitioning into resolved, resolved subfilter-scale, and subgrid-scale motions. The numerical error region is also shown above the dotted line. The grid is indicated by the vertical dashed line at wave number k_g (corresponding to the minimum resolvable wavelength); the explicit spatial filter is shown by the curved dashed line.

motions that are between the filter and grid cutoffs and hence are resolvable on the grid. These resolved subfilter-scale (RSFS) motions can be reconstructed by an inverse filter operation; however, the reconstruction is limited by numerical errors that increase near the grid cutoff. The portion to the right of the vertical dashed line contains subgrid-scale (SGS) motions that cannot be resolved on the grid and must be modeled.

The governing LES equations are given here with the usual meanings for the variables:

$$\frac{\partial \bar{u}_i}{\partial t} + \bar{u}_j \frac{\partial \bar{u}_i}{\partial x_j} = -\frac{1}{\rho} \frac{\partial \bar{p}}{\partial x_i} - g \delta_{i3} + \epsilon_{imn} f_n \bar{u}_m - \frac{\partial \tilde{\tau}_{ij}}{\partial x_j}$$

$$\frac{\partial \bar{u}_i}{\partial x_j} = 0$$

[f is the Coriolis parameter used in the atmospheric-scale simulations.] The total SFS stress is

$$\tau_{ij} = \overline{u_i u_j} - \tilde{u}_i \tilde{u}_j$$

and it can be decomposed into resolved and unresolved portions:

$$\tau_{SFS} = \tau_{ij} = \overline{u_i u_j} - \tilde{u}_i \tilde{u}_j = \underbrace{(\overline{u_i u_j} - \tilde{u}_i \tilde{u}_j)}_{\tau_{SGS}} + \underbrace{(\tilde{u}_i \tilde{u}_j - \tilde{u}_i \tilde{u}_j)}_{\tau_{RSFS}}$$

The first pair of terms on the right is the subgrid-scale stress which depends on scales beyond the resolution domain of the LES and contains the nonlinear leading term which must be modeled. The last pair of terms is the resolved filtered-scale stress which depends on the differences between the exact and filtered velocity fields within the resolution domain and can be reconstructed from knowledge of the resolved flow variables.

Using these concepts, Chow (2004) and Chow et al. (2005) implemented reconstruction approaches for the subfilter-scale stresses, modeled the subgrid-scale stresses, added a model for near-wall effects at rough boundaries, and then solved a range of flow cases. They are discussed below. Standard turbulence closures for large-eddy simulations based on finite-difference or finite-volume codes use isotropic eddy-viscosity models and hence ignore the contribution of the resolved subfilter-scale stresses as well as any anisotropy at the subfilter scales.

Combining reconstruction and eddy-viscosity models yields a sophisticated (and higher-order) version of the well-known mixed model of Bardina et al. (1983); the explicit filtering and reconstruction procedures clearly delineate the contribution of the RSFS and SGS motions. The reconstruction of the resolved subfilter-scale stress is accomplished either by a Taylor-series expansion to represent the velocity in the resolved and RSFS regions [Fig. 1] or by recursive filtering (Stolz et al., 2001) which leads to a series representation of that velocity field [the approximate deconvolution method]. Each approach therefore can be carried to higher orders of accuracy by including more terms in their respective series. The subgrid stresses are modeled with the Smagorinsky, dynamic Smagorinsky [DSM], or dynamic Wong-Lilly [DWL] models (Smagorinsky, 1963; Germano et al., 1991; Wong and Lilly, 1994).

The near-wall stress model is implemented to supplement the turbulence models and account for the stress induced by filtering near a solid boundary as well as the effect of the large grid aspect ratio. This model is based on the model of Brown et al. (2001) and essentially adds a drag to the flow there to mimic

the roughness and grid aspect ratio effects. The resulting stress appears as

$$\tau_{i, near-wall} = - \int C_c a(z) |\bar{u}| \bar{u}_i dz$$

Nakayama and Sakio (2002) and Nakayama et al. (2004) have provided a theoretical basis for this near-wall model for rough boundary flow.

2. Strategy of this paper

In what follows we examine a set of numerical simulations in the context of the above simulation approach to learn under what conditions the simulations are successful and what processes appear to dominate. We are most interested in the level of reconstruction needed in each case and the improvements made by the advanced turbulence models in the results obtained. We report on a pattern of results that show that the larger the scale of the flow the more external factors become important. This is a result of the change in boundaries from smooth in laboratory cases to rough for large, field cases and the effects of topography in some of our simulations.

The cases examined are turbulent channel flow with smooth walls at laboratory scale, neutral atmospheric boundary layer flow, simulations over an isolated hill, and flow in a steep Alpine valley.

3. Turbulent channel flow

Turbulent channel flow simulations were performed using second- and fourth-order finite difference codes for smooth walls in a rectangular straight channel (Gullbrand and Chow, 2003). Periodic boundary conditions were applied in the streamwise and spanwise homogeneous directions, with no-slip conditions at the top and bottom channel walls. A fixed mean pressure gradient was used to drive the flow. The Reynolds number based on the friction velocity was 395 and the computational domain was $(2\pi h, 2h, \pi h)$ in (x, y, z) where x is the streamwise direction, y the wall-normal direction, z the spanwise direction, and h is the half-height of the channel.

A systematic comparison of the LES results for different grid resolutions, finite difference schemes, and several turbulence closure models was performed; no near-wall model was required for the smooth walls. Explicit spatial filtering introduces resolved subfilter-scale as well as subgrid-scale turbulence terms. The dynamic Smagorinsky model [DSM] and the dynamic mixed model [DMM; Zang et al. (1993), Vreman et al. (1994)] were studied in this explicit filtering context, and a new dynamic reconstruction model [DRM] was introduced. The DRM combined the reconstruction procedure of the approximate deconvolution method (ADM, Stolz et al. 2001) with the dynamic Smagorinsky model for the SGS terms. Increasing the reconstruction levels for the RSFS stress improved the mean velocity as well as the total turbulent stress representation as illustrated in Figs. 2 & 3. For the DRM, the appended number [e.g., DRM5] signifies the number of terms retained in the reconstruction series, with a higher number indicating more accuracy in the RSFS representation.

4. Neutral atmospheric boundary layer flow

To further test the performance of DRM, we used the Advanced Regional Prediction System [ARPS], a compressible nonhydrostatic, terrain-following code (Xue et al., 2000 & 2001) to simulate a rotation-influenced neutral atmospheric boundary layer flow over flat, but rough, terrain. Using scale analysis, Blackadar and Tennekes (1968) showed that the near-wall region

of the resulting turbulent Ekman layer should follow a logarithmic law. Typical eddy-viscosity models do not give a good logarithmic region near the wall, usually over predicting the shear in the model so that the velocity is too low at the wall,

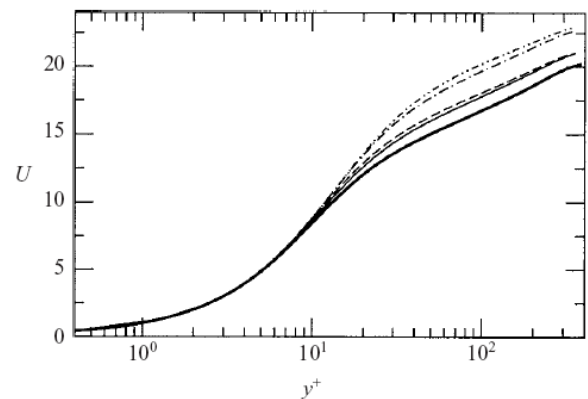


Fig. 2 Mean velocity profiles for the fourth-order code (64,49,48 grid points) with explicit filtering: - • - DSM; - • - DMM; - - - DRM5; — DRM10; and — DNS.

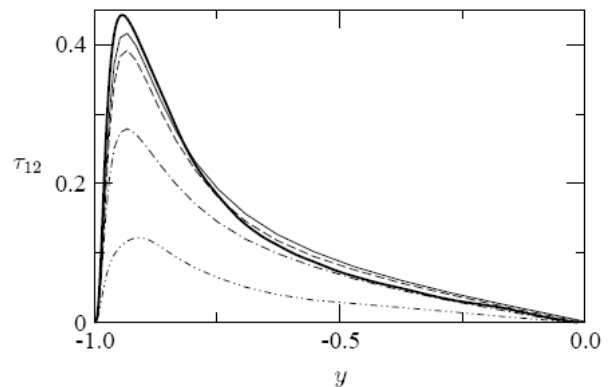


Fig. 3 Profiles of the turbulent stress τ_{12} for the fourth-order code (64,49,48 grid points) with explicit filtering: - • - DSM; - • - DMM; - - - DRM5; — DRM10; and — DNS.

and too high further away. The domain was about 1300 m in each horizontal direction with grid spacings of 32 m. In the vertical, a stretched grid was used, with 10 m spacing near the bottom and up to 65 m near the top of the domain, giving an average spacing of 37.5 m and a domain height of 1500 m.

The combined dynamic reconstruction model and near-wall stress model showed excellent agreement with similarity theory logarithmic velocity profiles (Fig. 4), a significant improvement over standard eddy-viscosity closures. Stress profiles also exhibited the expected pattern as seen in Fig. 3 for the turbulent channel flow: the total SFS stress increases with increasing reconstruction level (Fig. 5), approaching the result from a much finer resolution simulation. The largest contribution comes from the lower-order terms in the reconstruction series.

5. Simulations over an isolated hill

ARPS large-eddy simulations of flow over Askervein hill, an isolated hill in Scotland, were compared (Chow, 2004; Chow and Street, 2004) to the field observations of Taylor and Teunissen (1987). This flow was a challenging test for the reconstruction turbulence models which gave improved results for neutral boundary layer flow over flat terrain. This was the first time, to our knowledge, that reconstruction (scale-similarity) or dynamic turbulence models were applied to full-scale simulations of the atmospheric boundary layer over terrain.

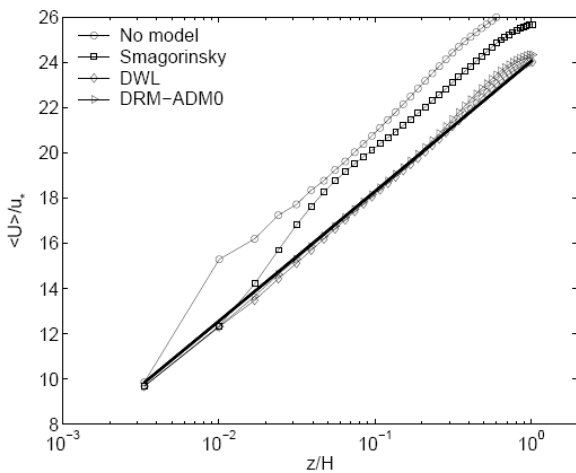


Fig. 4 Comparison of mean wind speed profiles for no turbulence model, the Smagorinsky model, the dynamic Wong-Lilly model, and for the DRM-ADM0 hybrid model (level-0 reconstruction, DWL, and near-wall stress). ADM refers to the approximate deconvolution model of Stolz et al. (2001). The theoretical log profile is shown with a solid line.

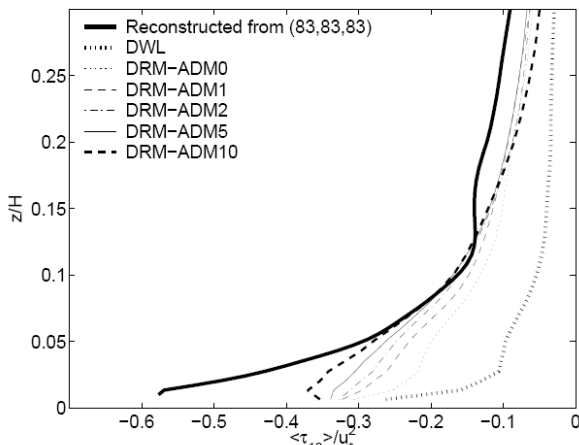


Fig. 5 Turbulent stresses computed *a posteriori* from velocity fields reconstructed from a fine resolution simulation (reconstructed from (83,83,83)), and the sum of RSFS and SGS stresses computed by coarse grid simulations (43,43,43): DWL, DRM-ADM0, DRM-ADM1, DRM-ADM2, DRM-ADM5, and DRM-ADM10. The near-wall stress contribution is not included. [Averaged over 100 000 to 120 000 s.]

Simulations with the lowest level of reconstruction (DRM-ADM0) were straightforward and showed improvement for wind speedup-ratios (ΔS) over the hill, when compared to results from the standard TKE-1.5 model (Fig. 6). The speed-up is a nondimensional measure often used in wind engineering for siting of wind turbines and is defined

$$\Delta S = \frac{S(z) - S_{RS}(z)}{S_{RS}(z)}$$

where S is the horizontal wind speed and S_{RS} is at the reference site where the input turbulent velocity profile is prescribed based on the field data. All the models under predicted the speed-up at the hill top, with the TKE-1.5 results slightly better than the rest. The under prediction at the hill top was likely caused by the fact that the peak elevation was slightly underestimated on our grid

(at 122 m, because of the grid spacing) compared to the actual elevation (126 m). The greatest difference among the models was, however, in the lee of the hill, where intermittent separation was observed in the field (Raithby et al., 1987). The TKE-1.5 model failed to produce the observed flow deceleration, whereas the DWL and particularly the DRM-ADM0 results were much better.

Predictions of total turbulent kinetic energy were also improved using the DRM (Fig. 7). Results were not as clear for the uw and vw stress components (not shown). Increased levels of reconstruction (beyond level 0) presented difficulties and required modification of the closure model near the ground. This was in part because the dynamic procedure under predicts the stress near the wall over rough surfaces. While all of the simulations using reconstruction also included an enhanced near-wall stress model, this was not sufficient to prevent instabilities. We adopted the hybrid approach of Iizuka and Kondo (2003), using the static Smagorinsky model in the lowest levels near the wall and the dynamic approach above. The specification of this static Smagorinsky layer was based on profiles of the dynamic eddy viscosity; however, the appropriate transition level from static to dynamic requires further study. The results, though promising, show that problems with the behavior of closure models in this sensitive near-wall region of the flow have not been completely solved.

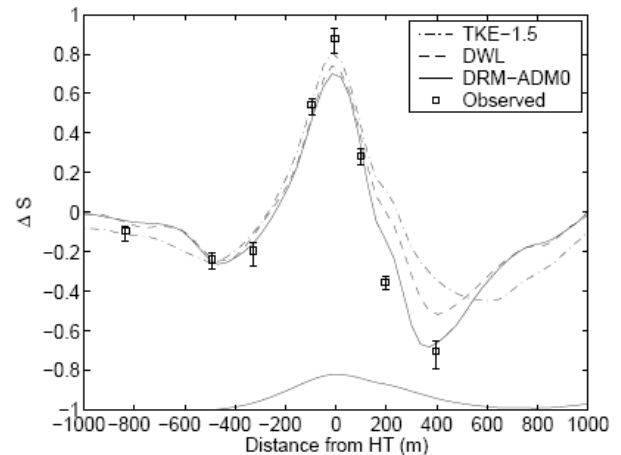


Figure 6: Comparisons of observed velocity speed-up along a line over the hill to simulated values using TKE-1.5, DWL and DRM-ADM0 closures. The profile of the hill is shown along the bottom axis.

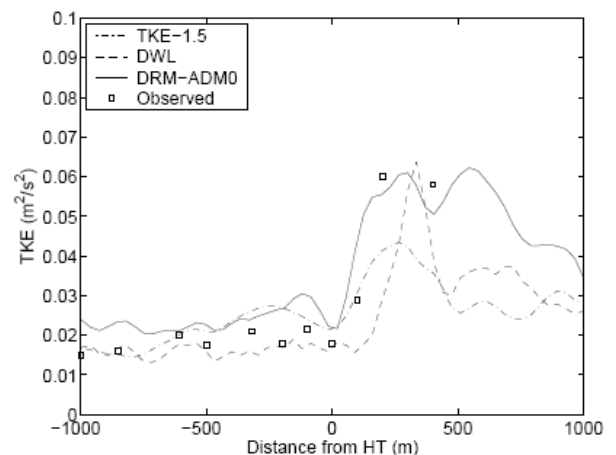
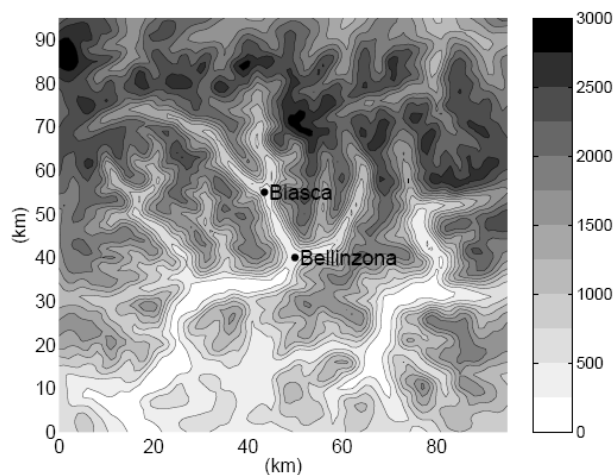


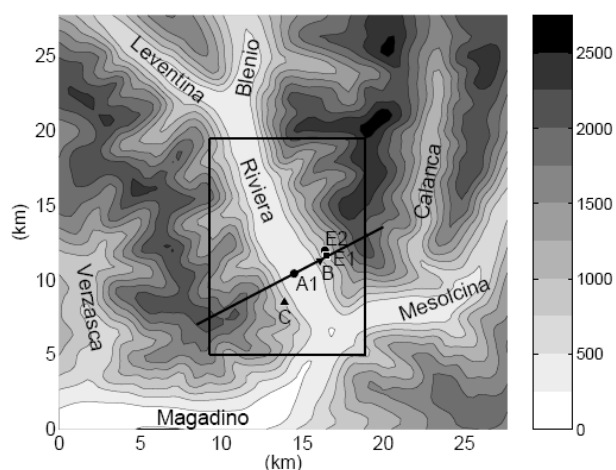
Fig. 7 Comparisons of observed TKE stress simulated values using TKE-1.5, DWL and DRM-ADM0 closures.

6. Flow in a steep Alpine valley

We investigated the steps necessary to achieve accurate simulations of flow over steep, mountainous terrain. Large-eddy simulations of flow in the Riviera Valley in the southern Swiss Alps were performed with ARPS at horizontal resolutions as fine as 150 m over a 30-hour period that coincided with observations during the MAP-Riviera project field campaign (Chow et al., 2005, and Weigel et al., 2005). In these simulations we employed forced lateral boundaries [from ECMWF forecasts] and one-way self-nested grids with resolutions ranging from 9 km to 150 m (Fig. 8). Vertical resolutions were as fine as 50 m on the largest grid and 20 m on the smallest one.



(a)



(b)

Fig. 8 Riviera Valley elevation contours (m above sea level) for (a) the 1 km grid and (b) the 350 m grid with the 150 m grid shown within. Locations of some surface stations and a typical vertical cross-section are also shown.

Comparisons were made to surface station and radiosonde measurements from the MAP-Riviera project field campaign of 1999. Excellent agreement between simulations and observations was obtained, but only when high-resolution land surface datasets were used and when the nested grid configurations were carefully chosen. Simply increasing spatial resolution without incorporating improved surface data gave unsatisfactory results. The sensitivity of the results to initial soil moisture, land use data,

grid resolution, topographic shading, and turbulence models was explored. Even with strong thermal forcing, the onset and magnitude of the up-valley winds were highly sensitive to surface processes in areas which are well outside the high-resolution domain. In particular, the soil moisture initialization on the 1 km grid was found to be crucial to the success of the finer resolution predictions. High-resolution soil moisture and land use data on the 350 m resolution grid also improved results. The use of topographic shading improved radiation curves during sunrise and sunset, but the effects on the overall flow were limited because of the strong lateral boundary forcing from the 1 km grid where terrain slopes are not well resolved.

The influence of the turbulence closure was also limited because of strong lateral forcing and hence limited residence time of air inside the valley, and because of the stable stratification which limited turbulent stress to the lowest few hundred meters near the surface (Fig. 9). Thus, in this case the effect of different turbulence models is unclear. Simulations without a turbulence model were poor. Results with the dynamic reconstruction [DRM] approach, however, did not differ appreciably from the standard TKE-1.5 closure in comparisons over a 24-hour time period (not shown), perhaps because the turbulent stresses were only significant in the lowest 500 m near the surface. Strong forcing at the lateral boundaries may also limit the development of turbulent structures within the nested domains. When the effect of the lateral boundaries was removed by performing short-term (1-hour) simulations using the same initial and boundary conditions but different turbulence models, the results wind speed contours showed noticeable differences (Fig. 10). Total SFS stress magnitudes were also larger for the DRM compared to the TKE-1.5 case. Higher grid resolution would allow the representation of finer-scale motions and may improve the ability of the SGS turbulence models to contribute appropriately under stable stratification.

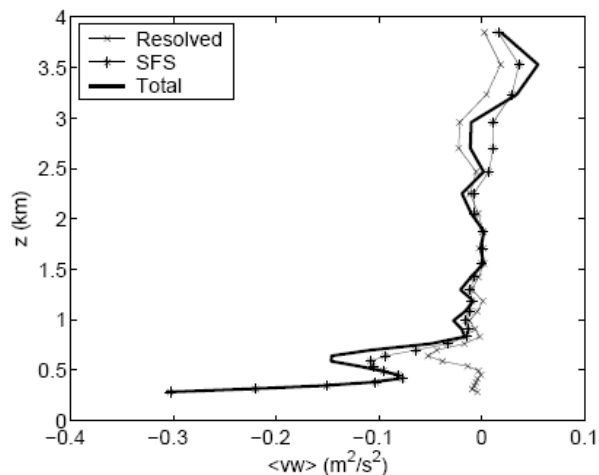


Fig. 9 Vertical profile of resolved, subfilter-scale, and total stress for $\langle vw \rangle$ [upvalley/vertical components] at the valley floor for the DRM turbulence closure). Time averaged between 1300 and 1500 UTC at 300 s intervals

7. Discussion

Large-eddy simulations of the atmospheric boundary layer are strongly influenced by the selection of the lower boundary conditions and turbulence models near the surface. In Chow (2004) and Chow et al. (2005) a new turbulence closure approach was presented and validated for a variety of turbulent flow applications. The method is based on scale partitioning which also accommodates the role of near-surface stresses for flow over rough surfaces. We have demonstrated that this approach is capable of providing significant improvements over traditional

methods. The resolved sub-filter scales can be reconstructed using a series expansion, while the subgrid-scale stresses must be modeled.

The first validation of this approach was for low Reynolds number channel flow (Sec. 3), where we found that increasing levels of reconstruction (for the RSFS component) improved the agreement with direct numerical simulation (DNS) results. The dynamic reconstruction model (DRM) combines reconstruction with a dynamic eddy-viscosity model. A significant discovery was that the SFS stresses grow with increasing reconstruction with the DRM, largely from the contribution of the RSFS components. The agreement with stresses extracted from DNS data was excellent.

aspect ratios near the wall. We use the DRM together with the near-wall stress model. This hybrid approach produced agreement with similarity theory through the reproduction of the expected logarithmic profile near the wall. The level of reconstruction affected the partitioning of the RSFS and SGS stresses, with the RSFS (and total SFS) contributions increasing with increasing reconstruction level, as seen in the channel flow simulations in Sec. 3.

We next evaluated the performance of the DRM for flow over Askervein Hill in Scotland (Sec. 5). Field observations provided evidence of intermittent separation in the lee of the hill, which was not captured by simulations using standard closure models (e.g. TKE-1.5). The DRM results (with the near-wall stress model) did show the expected intermittent separation and hence improved agreement with time-averaged measurements of flow speed-up over the hill. The Askervein simulations also demonstrated that inclusion of terrain created difficulties. Increasing levels of reconstruction could only be accommodated by removing the contribution of the dynamic model and replacing it with a static-coefficient Smagorinsky model in the lowest few levels near the wall. The reasons for the observed instabilities require future research on the behavior of stresses in the near-wall region.

The ultimate test for our turbulence modeling approach was performed in simulations of flow in the Riviera Valley in Switzerland (Sec. 6). Here, the steep terrain, heterogeneous surface conditions, and lateral boundary conditions pose severe challenges to any numerical simulation. The simulations required careful selection of appropriate surface datasets and boundary conditions. Results were particularly sensitive to soil moisture values. There was excellent agreement with observations at surface stations, soundings, and aircraft measurements. The use of the DRM (modified near the wall) in this valley flow was successful, but was overshadowed by differences in surface fluxes determined by the specification of surface characteristics. The lateral boundary conditions also largely determined the flow forcing; e.g. afternoon flow conditions in the 350 m nesting level were somewhat insensitive to small changes in the flow earlier in the day.

Given the improved results for atmospheric boundary layer simulations using the explicit filtering and reconstruction approach, it is clear that all LES codes will benefit from the inclusion of scale-similar terms in the turbulence model. Implementation of the series expansion models is straightforward. The dynamic eddy-viscosity model of Wong & Lilly (1994) is also simple to implement, but does require modifications near the surface for flow over complex terrain. These adjustments are not yet clearly understood, and may perhaps be addressed by consideration of improved near-wall stress models. Instead of the dynamic model, which can lead to instabilities over terrain, a constant coefficient Smagorinsky model or the TKE-1.5 closure can easily be used. These models require tunable coefficients, which are undesirable for general flows. The improved correlations and reconstruction of the RSFS stresses will, however, still be beneficial, particularly in improving the alignment of stress tensors and allowing for energy backscatter in the flow.

The sensitivity to surface boundary conditions has also been clearly shown in all the simulations from the neutral boundary layer (flat terrain) to the complex Riviera Valley flow. Much research is needed to construct a more robust near-wall stress representation (cf., Nakayama et al, 2004).

Acknowledgments: We gratefully acknowledge the support of a National Defense Science and Engineering Graduate fellowship [FKC] and National Science Foundation Grant ATM-0073395 (Physical Meteorology Program: S. Nelson, Program Director) [FKC and RLS]. Acknowledgment is also made to the National

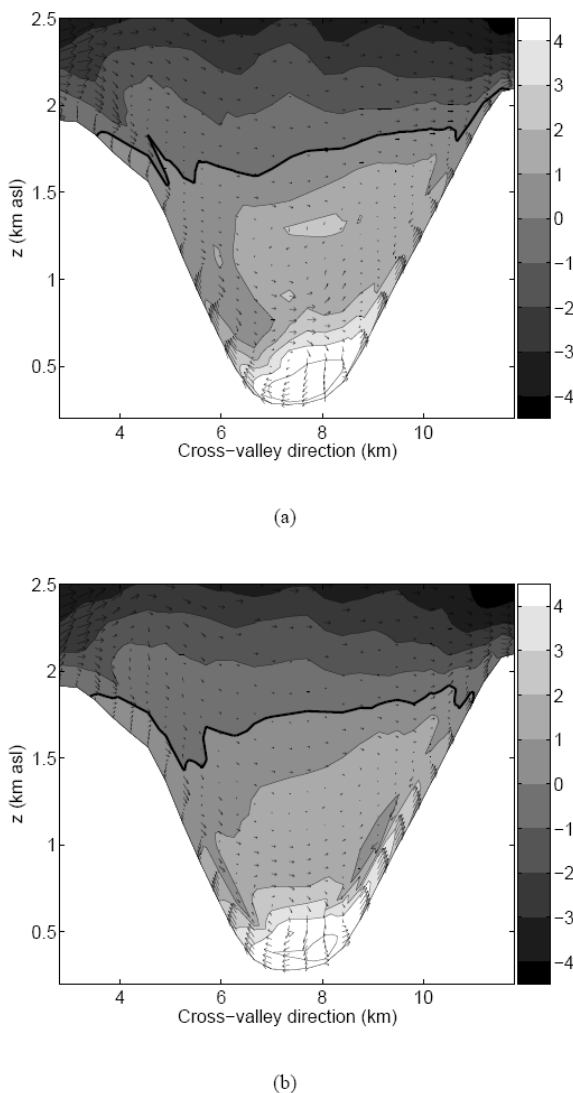


Fig. 10 Cross-valley winds (vectors) and along-valley winds (m/s, shaded) at 1300 UTC from the 350 m grid for (a) with TKE-1.5 and (b) with the DRM turbulence closure. Simulations start at 1200 UTC using identical initial and boundary conditions. The zero contour line is shown in bold.

When applied to neutrally-stratified atmospheric boundary layer flows (Sec. 4), the explicit filtering and reconstruction approach required augmentation from a near-wall stress layer. This enhanced stress layer represents the stresses induced by subgrid-scale surface roughness, poor resolution, and large grid

Center for Atmospheric Research, which is sponsored by NSF, for the computing time used in this research.

References

1. Andren, A., Brown, A.R., Graf, J., Mason, P.J., Moeng, C.-H., Nieuwstadt, F.T.M., and Schumann, U. Large-eddy simulation of a neutrally stratified boundary layer: A comparison of four computer codes, *Q. J. R. Meteorol. Soc.*, 120 (1994), pp.1457-1484.
2. Bardina, J., Ferziger, J. H. & Reynolds, W. C. Improved turbulence models based on large eddy simulation of homogeneous, incompressible, turbulent flows. Technical Report TF-19. Department of Mechanical Engineering, Stanford University, Stanford, California, (1983).
3. Blackadar, A. K. & Tennekes, H. Asymptotic similarity in neutral barotropic planetary boundary layers. *Journal of the Atmospheric Sciences* 25 (1968), 1015-1020.
4. Brown, A.R., Hobson, J.M, and Wood, N Large-eddy simulation of neutral turbulent flow over rough sinusoidal ridges. *Boundary-Layer Meteorology*, 98 (2001), pp. 411-441.
5. Carati, D., Winckelmans, G. S., and Jeanmart, H. On the modeling of the subgrid-scale and filtered-scale stress tensors in large-eddy simulation, *J. Fluid Mech.*, 441 (2001), pp. 119-138.
6. Chow, F.K. Subfilter-scale turbulence modeling for large-eddy simulation of the atmospheric boundary layer over complex terrain, Dissertation, Dept. Civ. & Env. Engrg., Stanford U., (2004), 349 pages.
7. Chow, F.K. and Street, R.L. Evaluation of turbulence models for large-eddy simulations of flow over Askervein Hill. 16th Symposium on Boundary Layers and Turbulence (2004), Paper 7.11.
8. Chow, F.K., Street, R.L., Xue, M., and Ferziger, J.H. Explicit filtering and reconstruction turbulence modeling for large-eddy simulation of neutral boundary layer flow. *Journal of the Atmospheric Sciences* 62 (2005), pp. 2058-2077.
9. Chow, F.K., Weigel, A.P., Street, R.L., Rotach, M.W., and Xue, M. High-resolution large-eddy simulations of flow in a steep Alpine valley. Part I: Methodology, verification, and sensitivity experiments. *Journal of Applied Meteorology*, (2005), in press. [See also: 11th Mountain Meteorology Conference, AMS, paper 6.2, 8 pages.]
10. Germano, M., Piomelli, U., Moin, P. & Cabot, W. H. A dynamic subgrid-scale eddy viscosity model. *Physics of Fluids*, 3 (1991), 1760-1765.
11. Gullbrand, J., & Chow, F. K. The effect of numerical errors and turbulence models in LES of channel flow, with and without explicit filtering, *Journal of Fluid Mechanics*, 495 (2003), pp. 323-341.
12. Iizuka, S. & Kondo, H. Large eddy simulations of turbulent flow over complex terrain. *Proceedings of the 11th International Conference on Wind Engineering* (2003), pp. 2689-2696.
13. Nakayama, A., and Sakio, K. Simulation of flows over wavy rough boundaries, *Annual Research Briefs, Center for Turbulence Research, NASA Ames/Stanford University*, (2002), pp. 313-324.
14. Nakayama, A., Hori, K., and Street, R. L. Filtering and LES of flow over irregular rough boundary. *Center for Turbulence Research, Proceedings of the Summer Program 2004* (2004), pp. 145-156.
15. Raithby, G. D., Stubble, G. D. & Taylor, P. A. The Askervein Hill project: a finite control volume prediction of three-dimensional flows over the hill. *Boundary-Layer Meteorology*, 39 (1987), pp. 247-67.
16. Smagorinsky, J. General circulation experiments with the primitive equations. *Monthly Weather Review*, 91 (1963), pp. 99-152.
17. Stolz, S., Adams, N. A. & Kleiser, L. An approximate deconvolution model for large-eddy simulation with application to incompressible wall-bounded flows. *Physics of Fluids*, 13 (2001), pp. 997-1015.
18. Taylor, P. A. & Teunissen, H. W. The Askervein Hill project: Report on the September/October 1983 main field experiment. Report MSRB-84-6. Atmospheric Environment Service, Downsview, Ontario (1985).
19. Vreman, B., Geurts, B. & Kuerten, H. On the formulation of the dynamic mixed subgrid-scale model. *Physics of Fluids* 6 (1994), pp. 4057-4059.
20. Weigel, A.P., Chow, F.K., Rotach, M.W., Street, R.L., and Xue, M. High-resolution large-eddy simulations of flow in a steep Alpine valley. Part II: Flow structure and heat budgets. *Journal of Applied Meteorology* (2005), in press.
21. Wong, V. C., and Lilly, D. K. A comparison of two dynamic subgrid closure methods for turbulent thermal-convection, *Physics of Fluids*, 6 (1994), pp. 1016-1023.
22. Xue, M., Droegemeier, K. K., and Wong, V. The Advanced Regional Prediction System (ARPS) - A multiscale nonhydrostatic atmospheric simulation and prediction tool. Part I: Model dynamics and verification, *Meteor. Atmos. Phys.*, 75 (2000), pp. 161-193.
23. Xue, M., Droegemeier, K. K., Wong, V., Shapiro, A., Brewster, K., Carr, F., Weber, D., Liu, Y., and Wang, D. H. The Advanced Regional Prediction System (ARPS) - A multiscale nonhydrostatic atmospheric simulation and prediction tool. Part II: Model physics and applications, *Meteor. Atmos. Phys.*, 76 (2001), pp. 134-165.
24. Zang, Y., Street, R. L. & Koseff, J. R. A dynamic mixed subgrid-scale model and its application to turbulent recirculating flows. *Physics of Fluids* 5 (1993), pp. 3186-3196.